Zahra, Tatheer, Jelvehpour, Ali, Thamboo, Julian A., & Dhanasekar, Manicka
(2020)
Interfacial transition zone modelling for characterisation of masonry under biaxial stresses.
Construction and Building Materials, *249*, Article number: 118735.

https://doi.org/10.1016/j.conbuildmat.2020.118735

Interfacial Transition Zone Modelling for Characterisation of Masonry under Biaxial Stresses

Tatheer Zahra[a], Ali Jelvehpour[a], Julian A Thamboo[b] and Manicka Dhanasekar[a,1]

[a] Queensland University of Technology, Brisbane, QLD 4000, Australia

[b] South Eastern University of Sri Lanka, Oluvil 32360, Sri Lanka

Abstract

This paper presents a concept of Interfacial Transition Zone (ITZ) enrichment for the characterisation of masonry under biaxial stress states to a nonlocal transient damage representative volume element (RVE) model developed by the authors (Jelvehpour et al, 2019). ITZ enrichment has been realised through a series of transition layers on either side of the unit - mortar interface with gradually varying properties of the constituent materials so that weaker mortar – stronger brick and stronger mortar – weaker brick combinations can be considered. Two model parameters, viz., the thickness and the stiffness degradation of the ITZ have been introduced to control the thickness and stiffness degradation of the transition layers; these parameters have been calibrated to fit the experimental data available in the literature. The calibrated ITZ enriched RVE model was then applied to conventional clay brick, concrete block and drystack (mortarless) masonry by simulating the experimental tests reported in the literature; good agreement was obtained. The RVE was then applied to predict the failure envelope of various masonry types subject to biaxial stress states. The ITZ enriched RVE eliminates the need for introduction of either interface element or contact nonlinearity between the masonry unit and the mortar or between drystack masonry units with wide ranging benefits of analysing masonry structures under various load cases.

Key Words: Interphases; Interfacial Transition Zone (ITZ); Transient-Gradient Damage; Representative Volume Element (RVE); Stiffness degradation; Conventional Masonry; Drystack Masonry.

---

[1] Corresponding Author: Prof. M. Dhanasekar, Queensland University of Technology, Brisbane QLD-4000, Australia. Ph. +61 7 3138 6666; email: dhanasekarmanicka@gmail.com

1 - Introduction

The authors recently reported a transient gradient damage model in the form of a representative volume element (RVE) for quasi-brittle bi-material composites, which is suitable for masonry applications (Jelvehpour et al, [1]). This model used a single-dissipative formulation of the isotropic damage in masonry incorporating a concept of variable Poisson's ratio in conjunction with a scalar damage definition. The model was shown to predict the strength of masonry reasonably well even when perfect bond between the mortar and the unit was enforced; however, stiffer responses were observed for the stress-strain predictions. To overcome the stiffer predictions, a concept of an interfacial transition zone (ITZ), inspired from the successful usages of ITZ in several multiphase materials and composites in the literature [2-10], is proposed in this paper. The ITZ essentially accounts for stiffness degradation of the weaker zone emanating from the physical interfaces between the constituents of the composites.

ITZ has been extensively used for more than two decades for the determination of the elastic properties of the cementitious composites such as concretes and mortar in the literature [2 – 14]; in all these articles, transitional layers between the aggregate inclusions and the cement matrix were formulated for the prediction of the elastic properties of the concretes. In the recent times, some advanced applications, such as the micro cracking and thermo-elastic field distribution have emerged [15, 16].

To the best of the knowledge of the authors, Giambanco and Mroz [17] appear to be the first to introduce the concept 'interphase' for masonry applications. Interphase is defined as a thin layer of a finite thickness (greater than zero) between two different materials assumed to have been bonded perfectly. Interface, on the other hand, refers to a zero-thickness boundary layer (or surface-to-surface contact interaction) between two materials with weak bonding properties [18 - 20]. Thus, within an ITZ, many interphases can be defined depending on the accuracy desired. Giambanco et al [21] and Scimemi et al [22] have further developed the interphase model into a finite element formulation and application to masonry structures respectively. In [17, 21, 22], only a single interphase between the surfaces of masonry units (i.e., the whole of the mortar layer) was considered. The novelty of the current paper is that it allows for gradual decrease in stiffness and strength of the transitional layers emanating on either side of the physical boundary between the two constituents (unit and mortar as in masonry – shown in Fig. 1). This novelty allows the ITZ proposed in this paper can account for weak mortar – strong brick or strong mortar – weak brick combinations and predict failure of either brick or mortar or both, whereas the works in [17, 21, 22] can only account for the weak mortar – strong brick combination (which is most common type of masonry). With the emergence of high bond strength masonry [18, 19, 23 – 26] and drystack masonry [27-29], it is timely to present a more generalised model such as the ITZ in this paper.

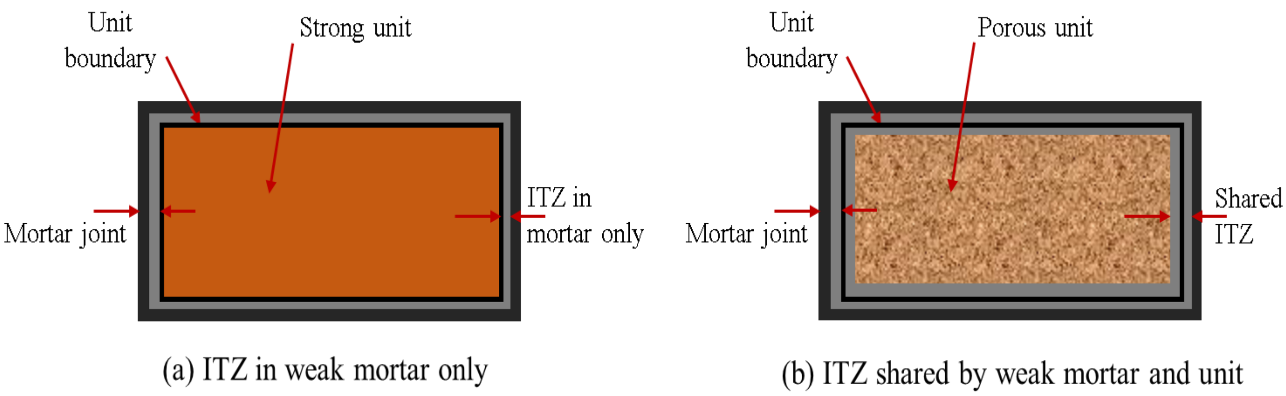

Figure 1: Representation of the Interfacial Transition Zone (ITZ) for masonry

Figure 1(a) shows the most common masonry containing strong bricks/ blocks/ stone units embedded within a surrounding weaker mortar layer - in such masonry ITZ would only exist in the weak mortar layer. In case of weak/porous masonry units, the ITZ would be shared between the units and mortar as shown in Figure 1(b). In high bond strength (usually in thin layer mortared masonry [23- 26, 35]), the ITZ may exclusively be in the unit (not illustrated in the figure). In the latter cases, both the units and mortar share damage due to similar strength and stiffness, for example in tuff stone masonry [30-31] or adobe masonry [32-33] built with mud mortar.

The idea of defining ITZ between the mortar and the unit through varying thickness and degrading stiffness of the ITZ was incorporated in the existing RVE damage model developed by Jelvehpour et al, [1].Utilising this concept can eliminate the need for the introduction of an interface element/ nonlinear contact concept between the two constituents which would add to the complexity of the model as was used in [18 - 20]. The sensitivity of this damage variable and the thickness of ITZ layers to the RVE was studied first and then the RVE was validated using experimental data for brick masonry from Dhanasekar [34], for block masonry from Barbosa et al, [36] and for drystack masonry from Oh et al, [37]. A good comparison was obtained and model results matched well with the experiments. The validated RVE was then employed to predict the biaxial failure envelope of masonry.

This paper is structured as follows: Enrichment of the RVE with an ITZ is discussed in Section 2. Sensitivity of ITZ parameters is presented in Section 3. Validation of ITZ enriched RVE under uniaxial loading is demonstrated in Section 4. The model application for predicting biaxial failure envelopes of various masonry types is discussed in Section 5. Conclusions and recommendations for further research are presented in Section 6.

2- Enrichment of the RVE with an Interfacial Transition Zone (ITZ)

Original RVE developed in [1] was based on the laws of classical damage mechanics principles of stiffness degradation of materials through $E=(1-\omega)E_o$, with ω as a scalar damage variable ranging from zero (undamaged material) to one (fully damaged material), in which E and E_o are the effective and the initial elastic modulus, respectively. The damage variable ω for the RVE is defined in the form of:

$$\omega=\begin{cases}1-\dfrac{\kappa_i}{\kappa}\left[(1-\alpha)+\alpha e^{-\beta(\kappa-\kappa_i)}\right] & if \quad I_1>0\\ \dfrac{\omega_c\zeta\kappa}{\omega_c\kappa-(\omega_c-\zeta)\kappa_c} & if \quad I_1\le 0 \;\; and \;\; \kappa\le\kappa_c\\ \dfrac{(\kappa-\kappa_c)+\omega_c(\kappa_c-\gamma)}{\kappa-\gamma} & if \quad I_1\le 0 \;\; and \;\; \kappa>\kappa_c\end{cases} \tag{1}$$

Where, α, β and ζ are material parameters, ω_c and κ_c are the threshold damage and threshold strain, respectively to control the damage commencement, κ_i is the threshold for damage initiation with κ as the maximum equivalent strain ε_{eq} at any loading instant and is expressed as given in Eq. (2) and parameter γ is defined as shown in Eq. (3).

$$\varepsilon_{eq}=\frac{(k-1)}{2k(1-2\upsilon)}I_1+\frac{1}{2k}\sqrt{\frac{(k-1)^2}{(1-2\upsilon)^2}I_1^2+\frac{12k}{(1+\upsilon)^2}J_2} \tag{2}$$

$$\gamma=\frac{\kappa_c\omega_c^2-2\zeta\kappa_c\omega_c+\zeta\kappa_c}{\omega_c^2-\zeta\omega_c} \tag{3}$$

In Eq. (2) and Eq. (3), k is the ratio between uniaxial compressive and tensile strength of the material, υ is the Poisson's ratio and I_1 and J_2 are the first invariant of the strain tensor and the second invariant of the deviatoric strain tensor, respectively. For drystack masonry an additional damage evolution law is introduced for initial seating behaviour of dry joints due to crushing of interstices or surface roughness in compression as given in Eq. (4).

$$\omega = \Phi\kappa^2 + S_j\kappa + I_0 \tag{4}$$

In which I_0 is the initial imperfection (unevenness) parameter between the units with a condition $0 \le I_0 \le 1$. The higher the joint surface unevenness I_0, the lower the contact between the two neighbouring units. When I_0 is equal to zero, the two neighbouring units are in full contact. Damage slope parameter S_j controls the rate of damage evolution in the joint closure due to crushing of interstices/unevenness under compressive loads. Parameter Φ in Eq. (5) controls the joint closure based on the level of strain in the joint represents as κ_{jc} compared with the threshold damage initiation strain κ_c for the unit.

$$\Phi = \begin{cases} \dfrac{\omega_c\zeta}{(\omega_c\kappa_{jc} - (\omega_c - \zeta)\kappa_c)\kappa_{jc}} - \dfrac{I_0 + S_j\kappa_{jc}}{\kappa_{jc}^{\;2}} & if \quad \kappa_{jc} \le \kappa_c \\ \dfrac{(\kappa_{jc} - \kappa_c) + \omega_c(\kappa_c - \gamma)}{(\kappa_{jc} - \gamma)\kappa_{jc}^{\;2}} - \dfrac{I_0 + S_j\kappa_{jc}}{\kappa_{jc}^{\;2}} & if \quad \kappa_{jc} > \kappa_c \end{cases} \tag{5}$$

The model is non-localised by introducing a transient gradient formulation as shown in Eq. (6).

$$\frac{\bar{\varepsilon}_{eq}}{\mu} - \nabla^2\bar{\varepsilon}_{eq} = \frac{\varepsilon_{eq}}{\mu} \tag{6}$$

In which ε_{eq} and $\bar{\varepsilon}_{eq}$ are the local and nonlocal equivalent strains, respectively and μ is the transient gradient parameter - expressed in Eq. (7), with a condition $\mu \neq 0$.

$$\mu = \begin{cases} c_0 + (c - c_0)\left(\dfrac{\bar{\varepsilon}_{eq}}{\varepsilon_\mu}\right)^{n_\mu} & \bar{\varepsilon}_{eq} \le \varepsilon_\mu \\ c & \bar{\varepsilon}_{eq} > \varepsilon_\mu \end{cases} \tag{7}$$

In the above equation, ε_μ is a limiting strain to mobilise the nonlocal interaction, n_μ is the nonlocal gradient parameter with c_0 as an arbitrary positive number selected so that at the initial time step, local and nonlocal strains remains the same between the integration points. All of the above-mentioned damage parameters and the transient-gradient parameters were calibrated in Jelvehpour et al, [1] using the experimental data of Thamboo et al, [23-26]. The details on the RVE modelling, periodic boundary conditions and meshing for application to masonry can be seen in [1]. This paper concentrates on enriching this RVE with ITZ.

The concept of ITZ enrichment in Figure 1 shows transitional layers possessing different properties in the RVE between the two constituents (mortar and unit). In traditional mortared masonries containing stronger clay brick or concrete block, the ITZ is assumed to commence from the edge of the unit and progresses into the mortar layer as shown in Figure 1(a). The cases where weak units are used (for example unburnt mud bricks) the ITZ layers are assumed to progress both into the unit and mortar as shown in Figure 1(b). In drystack masonry, interstices are analogised as mortar layer and the ITZ is assumed to exist as shown in Figure 1(b). All three cases have been analysed in this research.

The ITZ is divided into several layers (or, interphases, *1* to *n*) of varying properties for better simulation of damage in this zone as shown in Figure 2.

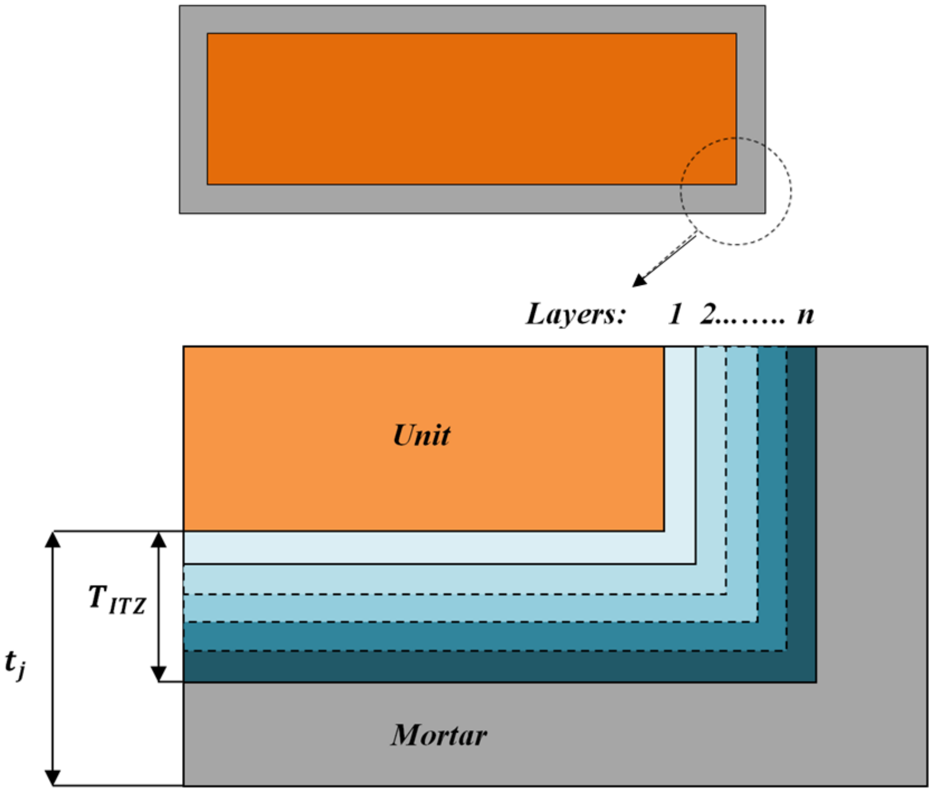

Figure 2: Division of ITZ into n layers

The strength and stiffness properties of these layers were allowed to gradually vary, from the weakest (highly damaged state) at the physical interface between the mortar and unit towards the strongest mortar layer. The maximum strength of this layer was set equal to the strength of mortar.

The properties of each layer within the ITZ vary based on the type and strength of the two materials that create bond. Numerous interface effects such as friction, distributed dislocations and delamination [38 – 40] further complicate the prediction of these properties for the ITZ layers. Depending on the materials considered and the thickness and the number of layers in the ITZ, different authors have considered different formulations for the properties of this zone in concretes [6, 9, 15, 41]. However, in this work for masonry RVE, a power law was introduced for the initial Young's modulus of each layer of the ITZ as presented in Eq. (8) to simulate reduced stiffness of the mortar-unit interface.

$$E_0(n) = E_M \left(\frac{(2n-1)(t_j - T_{ITZ}) + 2NT_{ITZ}}{2Nt_j} \right)^{\lambda_E} \tag{8}$$

Where,

n is the number of the specific layer from the interface between the two materials

N is the total number of layers within the ITZ

$E_0(n)$ is the initial Young's modulus of a specific layer

E_M is the Young's modulus of the mortar layer

t_j is the thickness of the mortar joint

T_{ITZ} is the thickness of the total ITZ and

λ_E is a parameter controlling the stiffness degradation.

From Eq. (8), it can be inferred that the stiffness of layers, and hence, the model predictions would be sensitive to thickness of ITZ, number of layers and stiffness degradation parameter λ_E. The sensitivity of these parameters to the model is discussed in the Section 3. The steps to simulate an ITZ enriched RVE are depicted in Figure 3 in the form of an algorithm.

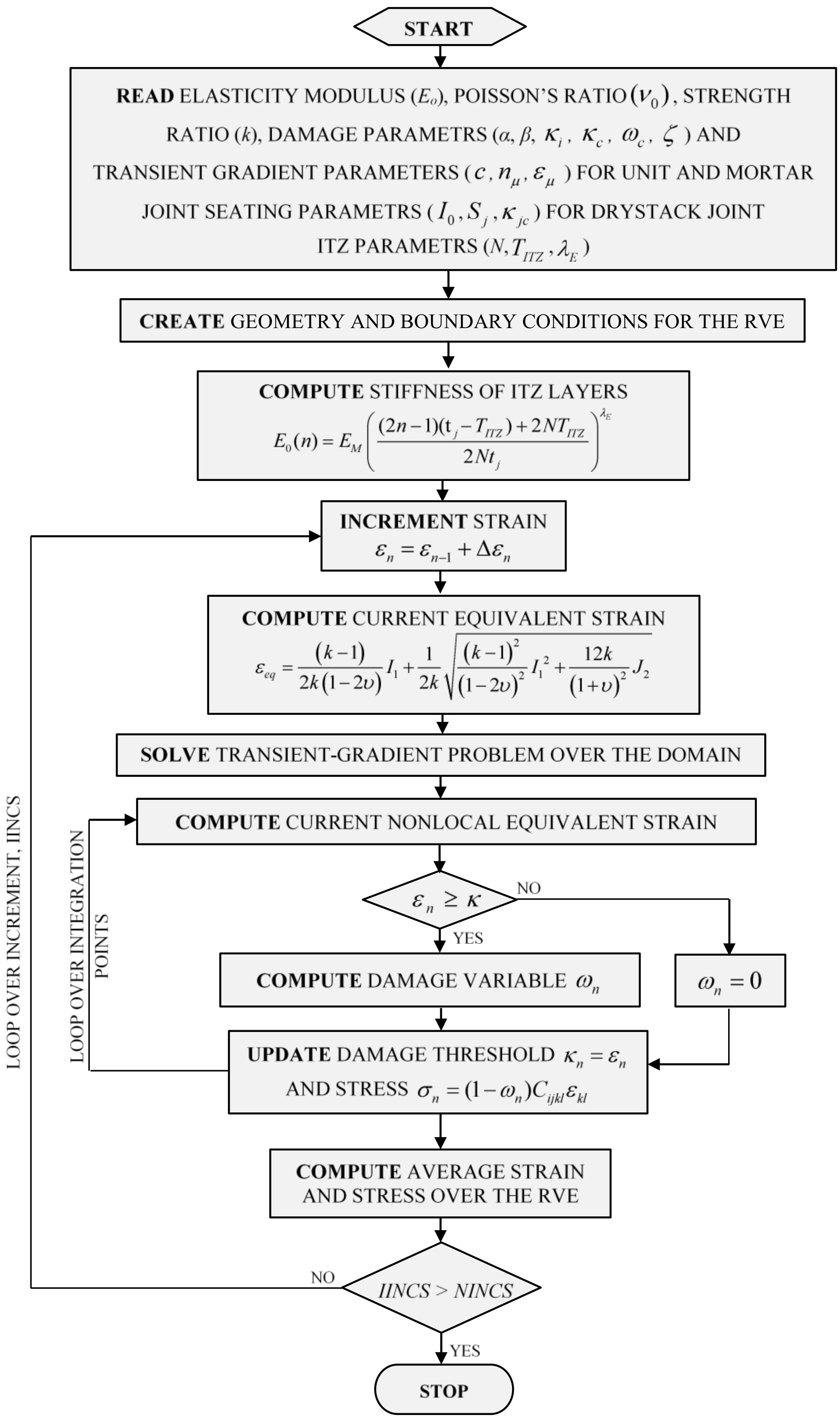

Figure 3: Algorithm to simulate ITZ enriched RVE

3. Sensitivity analysis of ITZ parameters

With a view to verifying the performance of the present ITZ enriched RVE, the effect of the ITZ parameters to the overall response of the system was examined. The RVE in Figure 4 was taken from Jelvehpour et al, [1]. The RVE was analysed under compression and tension perpendicular and parallel to bed joints as well as pure shear loading. The influences of overall thickness of the ITZ, thickness of the individual layers in ITZ and stiffness degradation parameter λ_E were considered in this sensitivity analysis. The elastic and damage parameters for brick and mortar used in this analysis are summarised in Table 1. This Table also shows the transient-gradient nonlocal properties, viz, the length factor (c), the limiting strain (ε_μ) and the gradient parameter (n_μ) of the constituents.

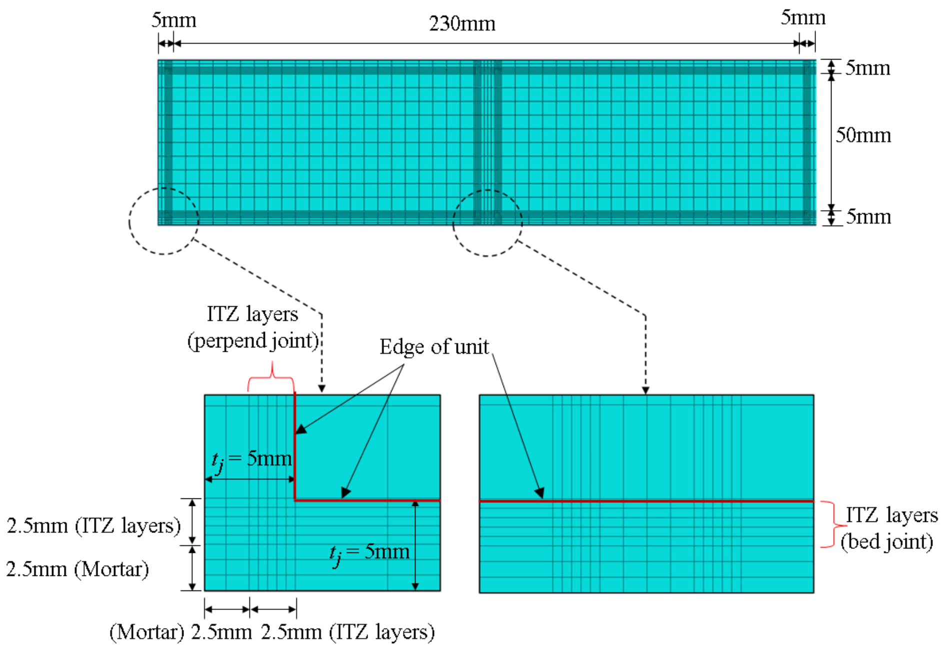

Figure 4: Finite Element discretisation of the RVE

Two-dimensional (2D) finite element analysis was carried out using reduced integration eight noded plane stress elements (CPS8R) to discretise the entire RVE. The finite element discretisation of the RVE is illustrated in Figure 4. The model could not be used with fully integrated elements, as the model could only solve the boundary value problem by taking an input of strain increment at a single integration point for each element in the mesh for the calculation of the corresponding output stress at that point as shown in algorithm in Figure 3. Therefore, reduced integration elements were required.

Table 1: Properties of the constituent materials

Property	Unit	Mortar
Eo (MPa)	15650	4000
ν_0	0.2	0.18
k	10	10
α	1.0	1.0
β	1000	1000
κ_i	0.00009	0.00012
κ_c	0.000162	0.00021
ω_c	0.4	0.4
ζ	-0.25	-0.25
c (mm^2)	5	5
n_μ	1	1
ε_μ	0.0009	0.0012

3.1 Effect of thickness of the Interfacial Transition Zone (ITZ) layers/ Interphases

In this section, the influence of the thickness of the Interfacial Transition Zone (ITZ) layers to the stress-strain behaviour of the masonry is discussed. For this purpose, five thicknesses (T_{ITZ}) were considered. The thickness of each layer (interphase) within the ITZ was kept constant (equal to 0.5 mm) in each of the five tests. The magnitude of the parameters selected for each test are presented in Table 2. Using these properties, Young's modulus for each transition layer was calculated from Eq. (8) and is listed in Table 3. A constant initial Poisson's ratio of 0.18 was considered for each layer of the ITZ.

Table 2: The ITZ parameters for each test

Test #	T_{ITZ} (mm)	t_j (mm)	N	λ_E
1	2.5	5	5	1.0
2	2.0	5	4	1.0
3	1.5	5	3	1.0
4	1.0	5	2	1.0
5	0.5	5	1	1.0

Figure 5(a) to 5(e) illustrates the influence of the ITZ layer thickness to the stress-strain behaviour of the masonry under uniaxial compression perpendicular and parallel to the bed joint, uniaxial tension perpendicular and parallel to the bed joint and pure shear, respectively.

Table 3: Stiffness of each transition layer of ITZ

Test #	E_M (MPa)	$E_0(1)$ (MPa)	$E_0(2)$ (MPa)	$E_0(3)$ (MPa)	$E_0(4)$ (MPa)	$E_0(5)$ (MPa)
1	4000	2200	2600	3000	3400	3800
2	4000	1900	2500	3100	3700	
3	4000	1667	2600	3533		
4	4000	1600	3200			
5	4000	1760				

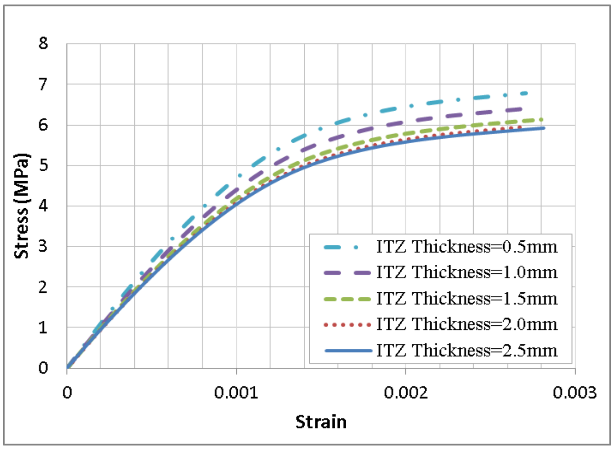

(a) compression perpendicular to bed joints

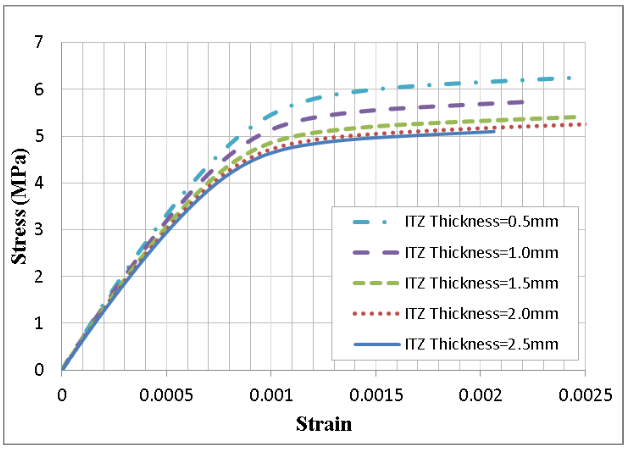

(b) compression parallel to bed joints

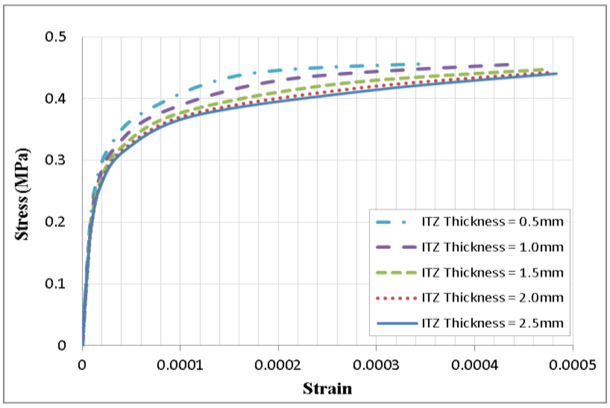

(c) tension perpendicular to bed joints

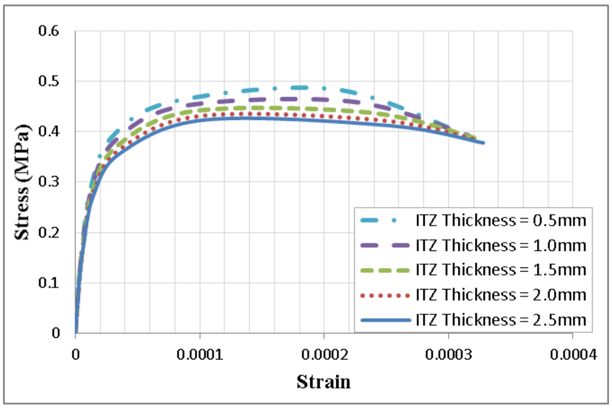

(d) tension parallel to bed joints

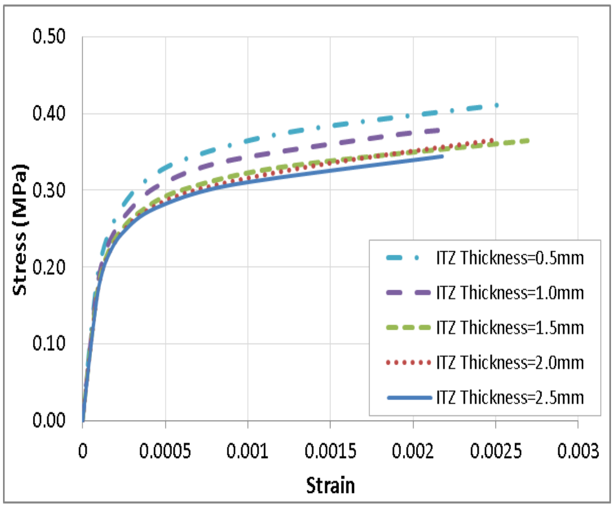

(e) Pure shear

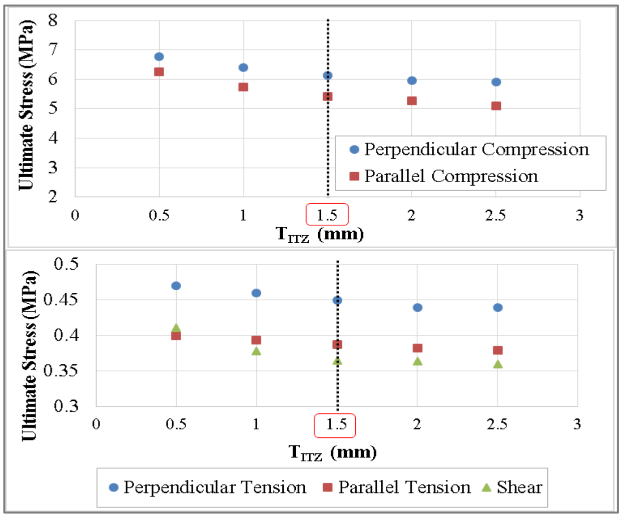

(f) Effect of T_{ITZ} on ultimate stress of masonry

Figure 5: Influence of ITZ thickness on stress-strain behaviour of the RVE

It can be observed that with the increase in the thickness of the ITZ, the response of masonry has softened, which is consistent to the logical expectation. Five thicknesses of ITZ were tested and similar observations can be seen on the effect of ITZ thickness for all loading cases depicted in Figure 5. Thickness of ITZ larger than 1.5mm has no significant effect on reducing the deformation and strength characteristics of masonry as shown in Figure 5(f). Thus, from this sensitivity analysis for the ITZ thickness effects, it can be concluded that a total thickness between 0.5 to 1.5mm is desirable for the ITZ with at least 5 layers within the ITZ.

3.2 Effect of stiffness degradation parameter λ_E

Influence of the ITZ stiffness parameter λ_E to the behaviour of masonry was investigated for five different cases. The magnitude of λ_E was varied from 0.5 to 4.0 as shown in Table 4; while all other parameters were kept constant. Based on the sensitivity analysis of ITZ thickness presented in the previous section, the total thickness of the ITZ was selected as 1.25mm divided into 5 layers (each layer was 0.25mm thick). A constant initial Poisson's ratio of 0.18 was considered for this analysis. The young's modulus of each layer was calculated from Eq. (8) for all ITZ layers for each test and is also presented in Table 4.

Figure 6(a) to 6(e) demonstrates the influence of the parameter λ_E to the ultimate stress of the masonry under uniaxial compression perpendicular and parallel to the bed joint, uniaxial tension perpendicular and parallel to the bed joint and pure shear for five different values. It can be observed in these figures that the larger the value of λ_E, the weaker the response of RVE. This behaviour is also obvious from Table 4, the higher the stiffness degradation parameter, the bigger the range of stiffness change within the ITZ.

Table 4: Properties of ITZ layers to study the effect of λ_E

Test #	λ_E	E_M (MPa)	$E_0(1)$ (MPa)	$E_0(2)$ (MPa)	$E_0(3)$ (MPa)	$E_0(4)$ (MPa)	$E_0(5)$ (MPa)
1	0.5	4000	2966	3225	3464	3688	3899
2	1.0	4000	2200	2600	3000	3400	3800
3	2.0	4000	1210	1690	2250	2890	3610
4	3.0	4000	665	1098	1687	2456	3429
5	4.0	4000	366	714	1266	2088	3258

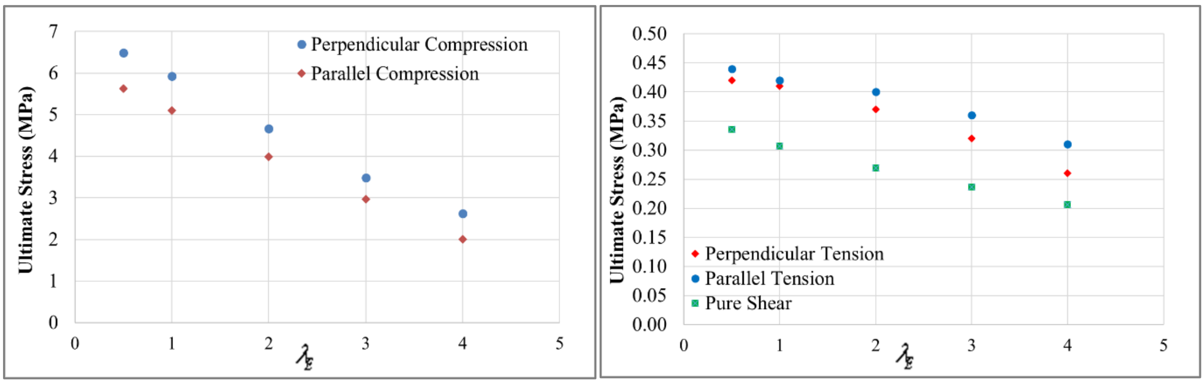

(a) Compression (b) Tension and shear

Figure 6: Influence of λ_E on the ultimate stress of masonry

It was determined through calibration for different types of masonry that a magnitude of $\lambda_E = 0.5$ fitted most of the available experimental data from the literature [23, 24, 29, 30]. In section 4, validation of Interfacial Transition Zone (ITZ) enhanced RVE is presented for a number of uniaxial experimental datasets available in the literature for conventional mortared and drystack masonry.

4. Validation of the ITZ enriched damage model of RVE

The predictions of the ITZ enriched RVE were validated using several experimental datasets reported in the literature and presented in this section. The validation was carried out for clay brick masonry, concrete block masonry and drystack masonry subjected to uniaxial loading.

4.1 Validation for traditional clay brick masonry

Dhanasekar et al [38] conducted tests on solid clay brick masonry samples made of half scale bricks having dimensions of 55 mm (width), 25 mm (height) and 115 mm (length) with a mortar joint thickness of 5 mm. The RVE was developed of the same dimensions as shown in Figure 7 to predict the behaviour under uniaxial compression and tensile loads. The damage model parameters and material properties were as listed in Table 1. The selected elastic modulus of each ITZ layer (shown in Figure 7) is listed in Table 5. The initial Poisson's ratio for all layers was considered as 0.18. Within the RVE a 1.25 mm ITZ was considered as shown in Figure 8. Each ITZ layer had a thickness of 0.25 mm and the stiffness degradation parameter was kept as $\lambda_E = 0.5$.

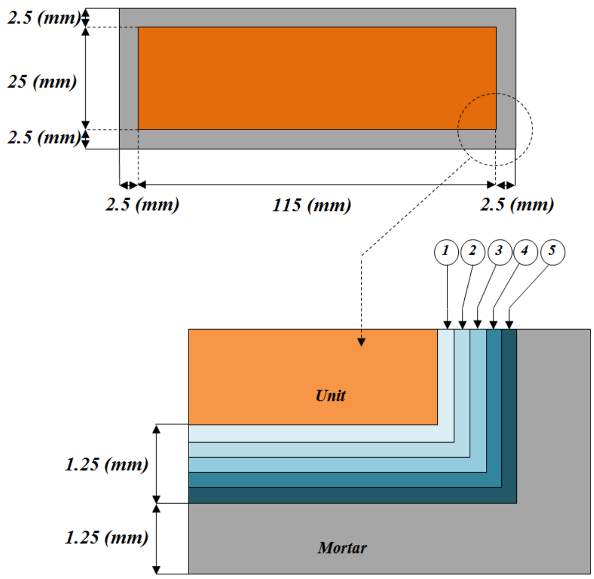

Figure 7: Dimensions of the modelled RVE and its ITZ for experiments conducted by Dhanasekar et al [42]

Table 5: Elastic Modulus of ITZ layers

$E_0(1)$ (MPa)	$E_0(2)$ (MPa)	$E_0(3)$ (MPa)	$E_0(4)$ (MPa)	$E_0(5)$ (MPa)
2200	2600	3000	3400	3800

Figure 8 shows the predicted stress-strain behaviour by the RVE compared with the experimental datasets for compression perpendicular and parallel to the bed joint as well as uniaxial tension perpendicular and parallel to the bed joint of samples. Globally good agreement was found for the model and experimental data. It can be observed from the above-mentioned tests that ITZ enriched RVE damage model can predict the stress-strain behaviour of clay brick masonry that closely matched to the experiments. However, it should be noted that a slight under-estimation of the final strength of the RVE can be seen in all cases, which is desirable for computational models as the predictions are conservative and can be used in design.

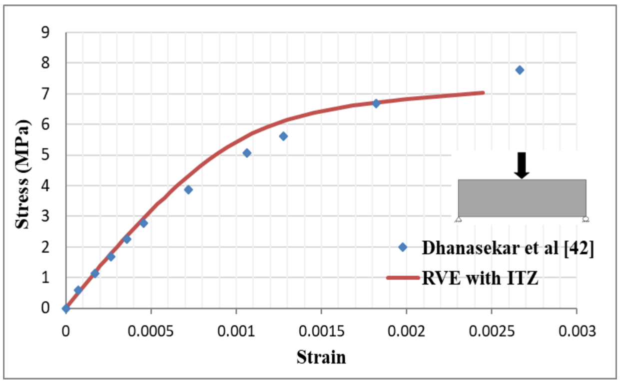

(a) compression perpendicular to bed joints

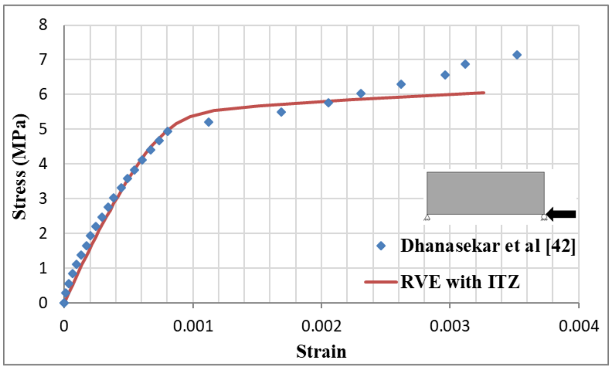

(b) compression parallel to bed joints

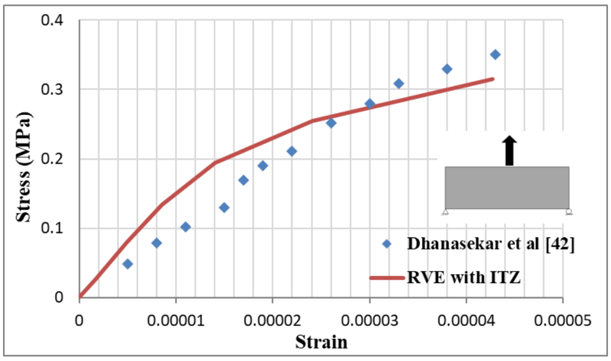

(c) tension perpendicular to bed joints

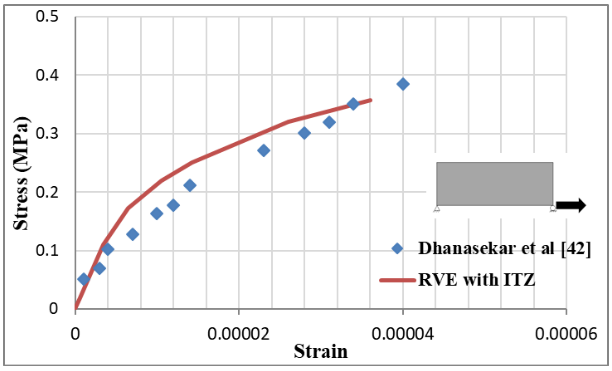

(d) tension parallel to bed joints

Figure 8: Comparison of the RVE predictions with uniaxial tests of Dhanasekar [42]

4.2 Validation for traditional concrete block masonry

Barbosa et al, [36] conducted a series of uniaxial compression tests on hollow concrete block prisms with four different unit strengths. The dimensions of the RVE modelled to represent their testing sample is shown in Figure 9. Their block dimensions were 140 mm (width), 190 mm (height) and 390 mm (length) bonded with a mortar joint thickness of 10 mm. Table 6 summarises the tested elastic properties of mortar and concrete blocks, considered for each prism test. An Interfacial Transition Zone (ITZ) with 5 layers was considered with 2.5 mm thickness as shown in Figure 9. Each ITZ layer had a thickness of 0.5 mm and the ITZ parameter was taken as $\lambda_E = 0.5$. For each of the four prism tests (P1, P2, P3 and P4), initial elastic modulus $E_0(n)$ of all ITZ layers was determined using Eq. (8) and was input in the RVE model.

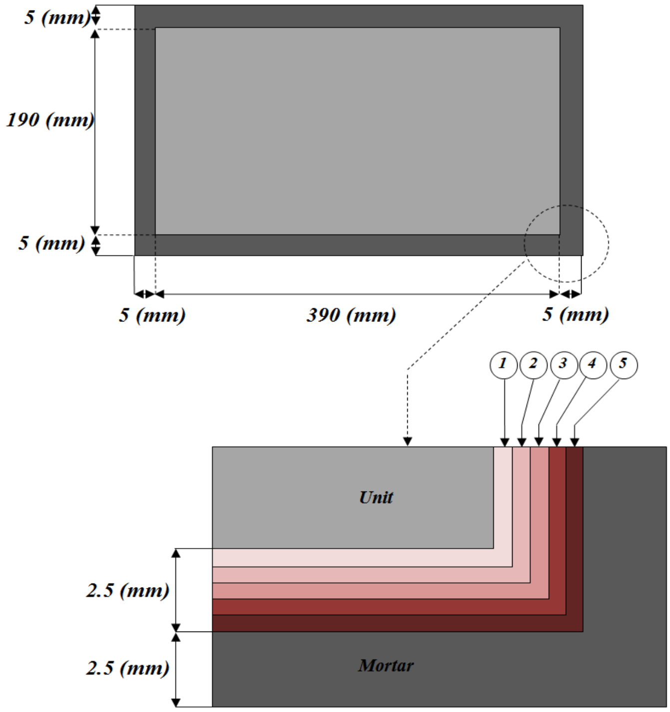

Figure 9: Dimensions of the modelled RVE and its ITZ for experiments conducted by Barbosa et al, [36]

Table 6: Properties of constituents for prisms tests of Barbosa et al, [36]

Parameter	P1		P2		P3		P4	
	Block	Mortar	Block	Mortar	Block	Mortar	Block	Mortar
E (MPa)	20595	9745	17449	8121	22175	13195	27104	16672
ν_0	0.203	0.127	0.195	0.134	0.204	0.151	0.207	0.153
k	10	9	11	9	10	9	12	10
α	1.0	1.0	1.0	1.0	1.0	1.0	1.0	1.0
β	1000	1000	1000	1000	1000	1000	1000	1000
κ_i	0.00011	0.00011	0.00011	0.00011	0.00011	0.00011	0.00011	0.00011
κ_c	0.00017	0.000165	0.000155	0.000165	0.00017	0.000165	0.00017	0.00025
ω_c	0.4	0.4	0.4	0.4	0.4	0.4	0.4	0.4
ζ	-0.25	-0.25	-0.25	-0.25	-0.25	-0.25	-0.25	-0.25
$c\ (mm^2)$	5	5	5	5	5	5	5	5

n_μ	1	1	1	1	1	1	1	1
ε_μ	0.0001	0.0001	0.0001	0.0001	0.0001	0.0001	0.0001	0.0001

The stress-strain behaviour of masonry under uniaxial compression perpendicular to bed joints was compared with the experimental data of Barbosa, et al. [36] as shown in Figure 10. Globally good agreement was observed for the model and experimental data. Moreover, the model predictions are conservative which is expected of the numerical models to ensure safety. The model favourably predicts the overall stress-strain behaviour of the masonry prisms under uniaxial compression.

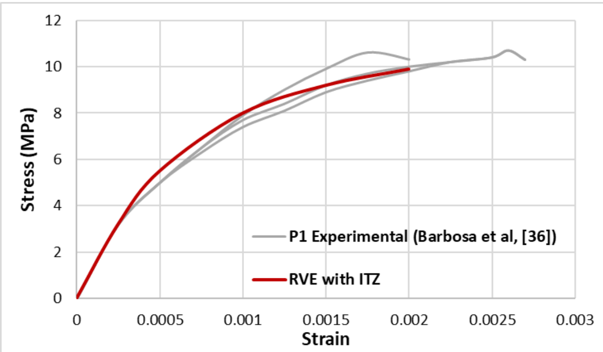

(a) P1

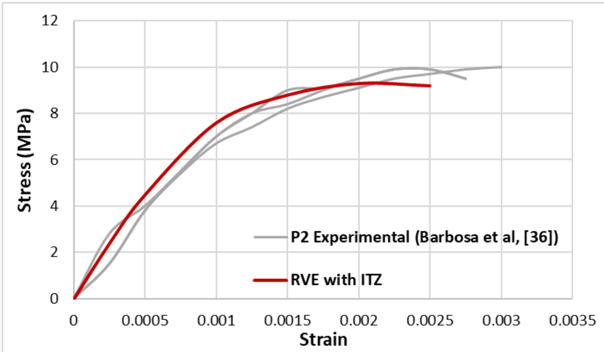

(b) P2

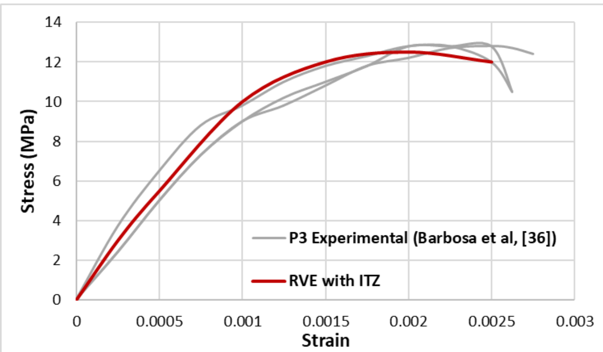

(c) P3

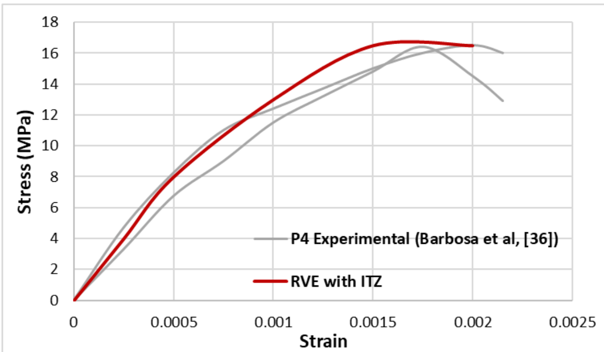

(d) P4

Figure 10: Comparison of the RVE predictions with the experimental tests of Barbosa et al, [36]

4.3 Validation for drystack masonry

The RVE was also validated with the experimental work reported by Oh et al, [37]. Two types of drystack blocks were used in this set of experiments: Interlocking blocks and modified H-blocks. The compressive strength of blocks was considered same as was mentioned in [37], all other model parameters and material properties were chosen based on the parametric studies conducted in [1] and section 3 of this paper and are listed in Table 7. The properties used for simulating the joint unevenness in the ITZ across the drystack unit namely: initial imperfection (unevenness) parameter (I_0), Damage slope parameter (S_j) and limiting damage strain in the joint (κ_{jc}) are also listed in Table 7.

Table 7: Input properties for drystack masonry

Properties	Modified H-Block	Interlocking Block
E (MPa)	21000	10000
ν_0	0.2	0.2
k	10	10
α	1.0	1.0
β	1000	1000
κ_i	0.00005	0.00005
κ_c	0.00023	0.0002
ω_c	0.4	0.4
ζ	-0.25	-0.25
I_0	0.5	0.9
S_j	-1000	-1000
κ_{jc}	0.0002	0.00018

The dimensions of the modified H-blocks were 136mm (Long) × 68mm (High) × 68mm (Thick) and for the interlocking blocks were 128mm (Long) × 64m (High) × 64mm (Thick). An idealised RVE modelled for these drystack prisms is presented in Figure 11. ITZ of total thickness of 2mm was considered all around the blocks to simulate the weak zone due to surface unevenness between the drystack bed and perpend joints. The ITZ was divided into 5 equal layers each of 0.4mm thickness as shown in Figure 11. The ITZ parameter was taken as

$\lambda_E = 0.5$. The RVE was analysed under uniaxial compression perpendicular to bed joints to simulate the experimental tests conducted by Oh et al, [37].

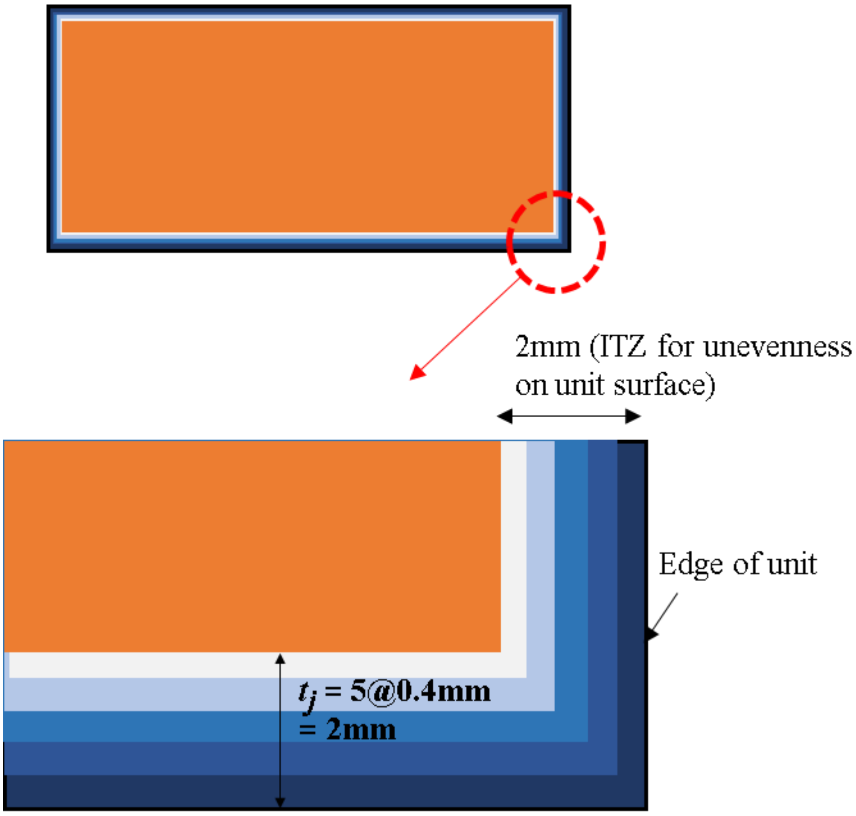

Figure 11: Modelled RVE and its ITZ for experiments conducted by Oh et al, [37]

The results for RVE simulations for modified H-block prisms and the interlocking block prisms are shown in Figures 12 and 13 respectively. From Figure 12 and 13 it can be concluded that RVE is able to predict the behaviour of drystack masonry with reasonable accuracy. The predicted stress-strain behaviour matches well with the experimental data with initial progressive seating behaviour of joints under compression due to crushing of interstices within the RVE controlled by introduced imperfection parameters.

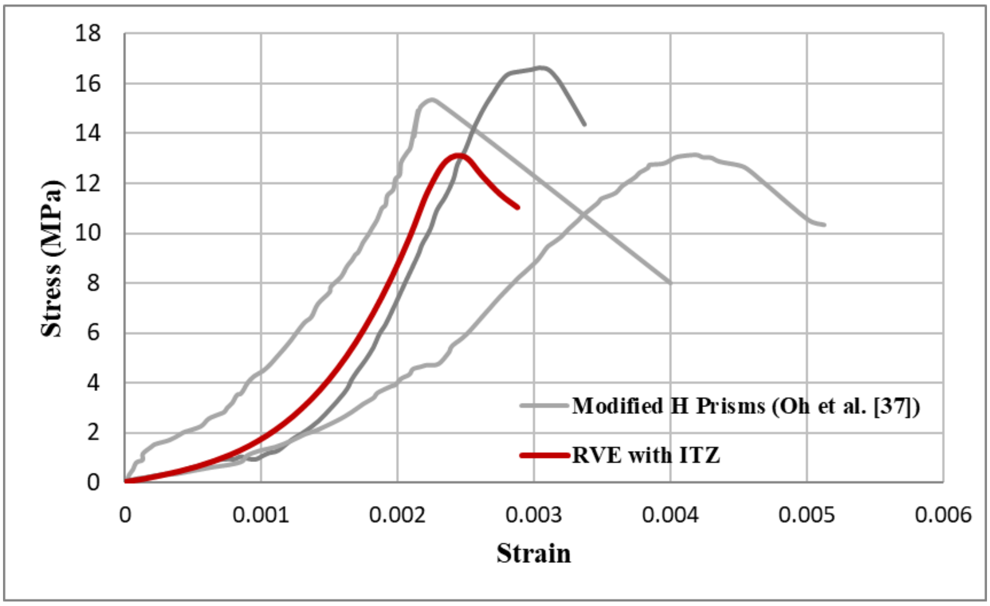

Figure 12: Validation results for modified H-Block prisms by Oh et al, [37]

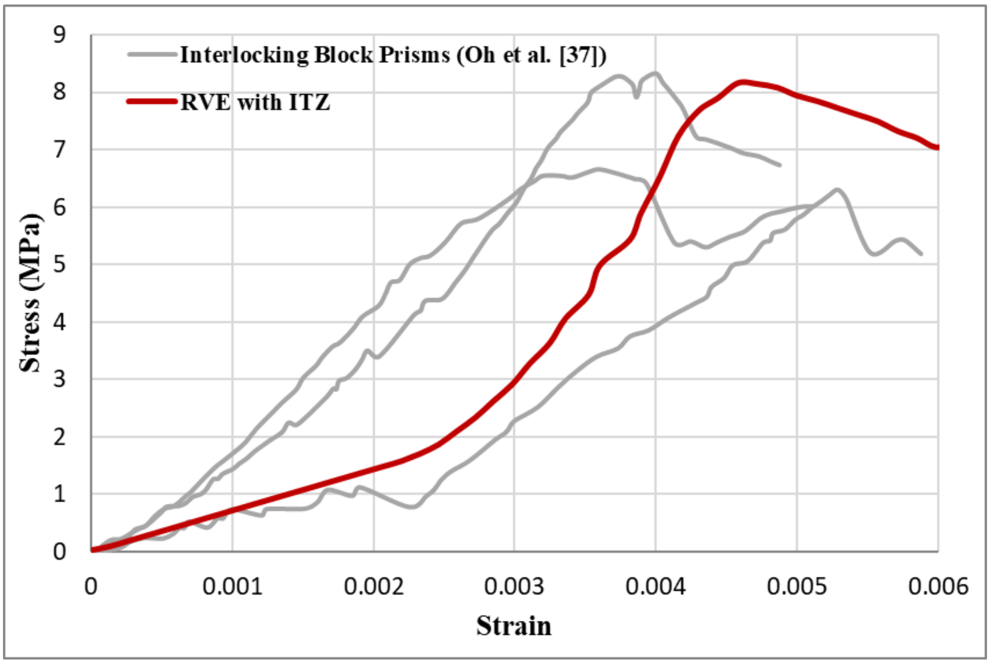

Figure 13: Validation results for the interlocking block prisms by Oh et al, [37]

5. Application of ITZ enriched RVE for predicting biaxial behaviour of masonry

From a phenomenological perspective, masonry is an anisotropic composite material in spite of its constituents can be regarded isotropic. This anisotropy is mainly due to the geometrical arrangements of units and mortar. Considering the anisotropy of masonry, the failure envelope for the in-plane stress state should be represented in terms of all plane stress components σ_x, σ_y and τ_{xy}, where x-axis considered parallel to the bed joints direction and y-axis parallel to the head joints direction. Alternatively, the failure envelope can also be represented in terms of the principal stresses and an angle θ which is the angle between the material axes and the principal axes as is shown in Figure 14.

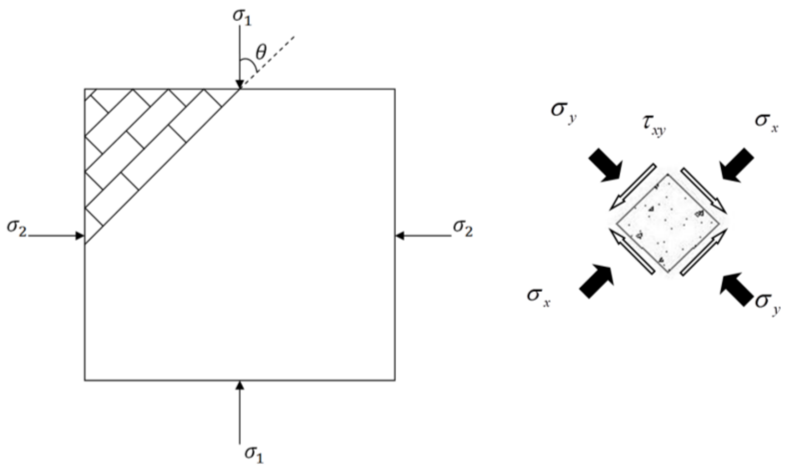

Figure 14: Representation of material and principal axes in masonry

The ability of the present RVE model to predict the failure envelope of conventional masonry under in-plane loading was demonstrated through a comparison with available experimental data of Dhanasekar et al, [42]. The considered loading configurations were uniaxial tension, uniaxial compression, biaxial tension-compression and biaxial compression-compression. In total 22 combinations for these stress states were simulated using the developed RVE model for bed joint angles of 0°, 22.5°, 45°, 67.5° and 90° to determine the principal stresses for each case. Table 8 illustrates these loading combinations which were applied to the RVE shown in Figure 15 for each bed joint orientation angle. Values shown in this table are the ratio between normal $(\sigma_1 = \sigma_n)$ and parallel loads $(\sigma_2 = \sigma_p)$ for each load case. Mohr circle of stress transformation was used to obtain the corresponding σ_{xx}, σ_{yy} and τ_{xy} for all loading combinations of Table 8. These loads are then applied to RVE with periodic boundary conditions as shown in Figure 15.

Table 8: Load factors for each load combination

Load Case	**1**	**2**	**3**	**4**	**5**	**6**	**7**	**8**	**9**	**10**	**11**
σ_n / σ_p	∞	0	∞	0	+1	+0.5	+0.25	+0.125	+0.083	+2	+4
Load Case	**12**	**13**	**14**	**15**	**16**	**17**	**18**	**19**	**20**	**21**	**22**
σ_n / σ_p	+8	+12	-4	-2	-1	-0.25	-0.5	-1	+1	+0.5	+2

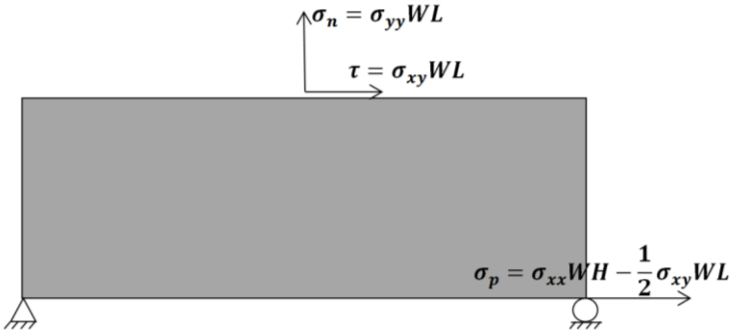

Figure 15: Biaxial Loading configuration and boundary conditions of the RVE

The material properties employed are shown in Table 1 and simulated RVE dimensions are shown in Figure 7 which were taken from Dhanasekar et al, [42]. A full failure envelope of masonry in the normal-parallel stress plane (principal plane) for the bed joint orientations of 0°, 22.5°, 45°, 67.5° and 90° to validate the experimental results of Dhanasekar et al, [38] is plotted in Figure 16. These results were then also verified by plotting the failure stress predicted by the ITZ enriched RVE of all of these cases against the experimental results presented by Dhanasekar et al, [42] for normal-shear stress plane and parallel-shear stress plane in Figures 17 and 18, respectively. Good agreement can be observed between the model's numerical predictions and the experimental datasets with slight under-estimation of strength which is desirable for design purposes [43 - 45].

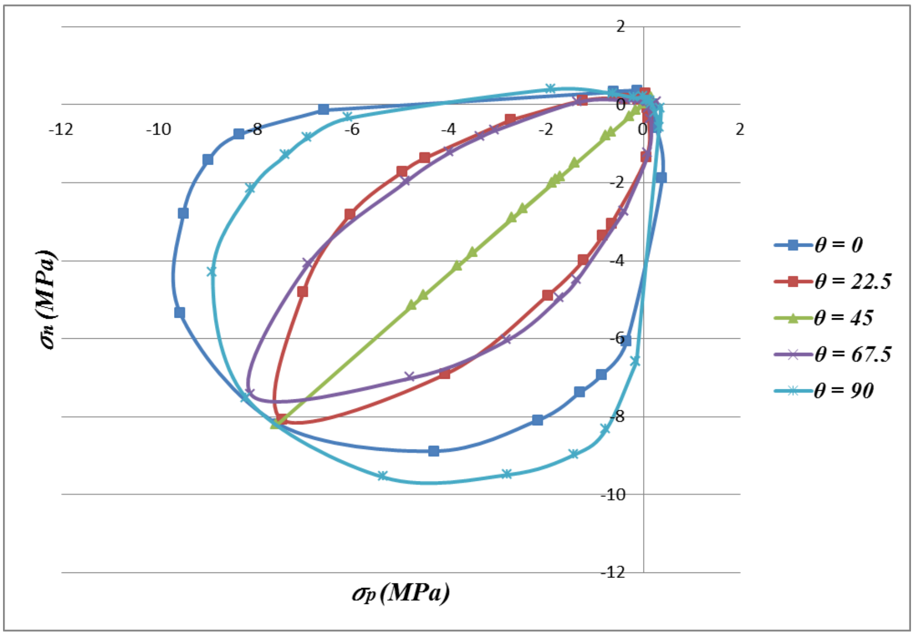

Figure 16: Biaxial failure envelope of the RVE in terms of principal stresses for bed joint angles 0°, 22.5°, 45°, 67.5° and 90°

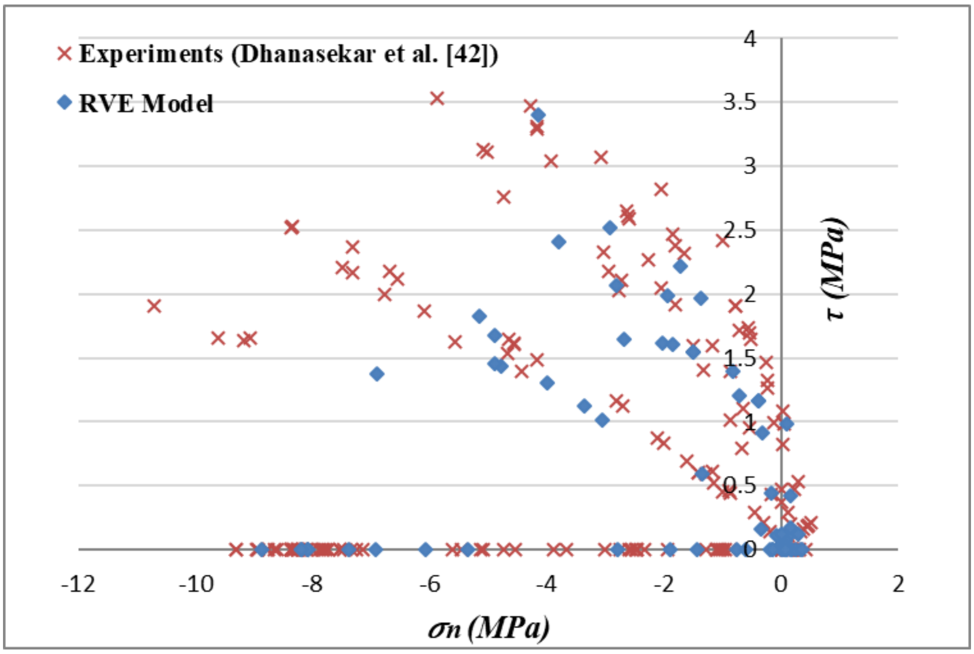

Figure 17: Failure envelope of the RVE in terms of shear stress τ and stress normal to bed joint σ_n for bed joint angles of 0°, 22.5°, 45°, 67.5° and 90°

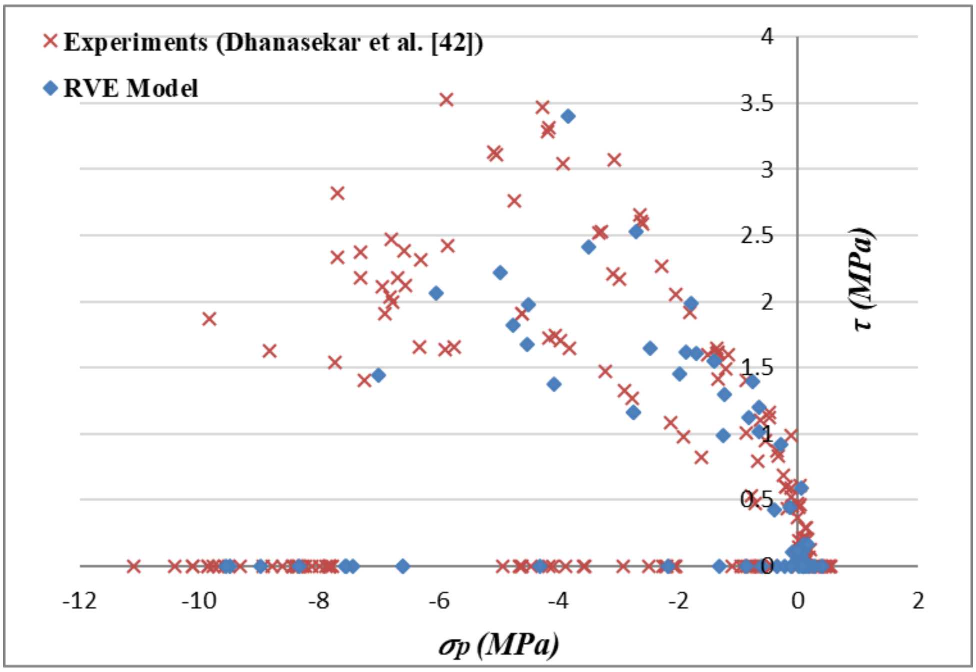

Figure 18: Failure envelope of the RVE in terms of shear stress τ and stress parallel to bed joint σ_p for bed joint angle of 0°, 22.5°, 45°, 67.5° and 90°

The capability of predicting in-plane behaviour of clay brick masonry from the developed ITZ enriched RVE has been proven from Figures 16, 17 and 18 with comparison to the experimental results of Dhanasekar et al, [42].

In order to predict the biaxial behaviour of concrete block masonry, the RVE developed for uniaxial compression testing in Section 5.2 (to validate Barbosa et al, [36] experiments) was employed and simulated for different biaxial principal stress ratios for orientation angles of 0° and 90°, which represents the case of zero shear. The results are shown in Figure 19 for all the four prisms P1, P2, P3 and P4 tested earlier in Section 4.2 under uniaxial compression.

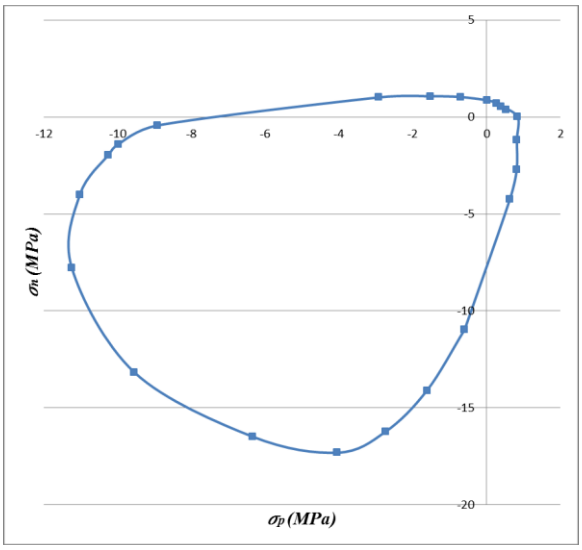

(a) P1

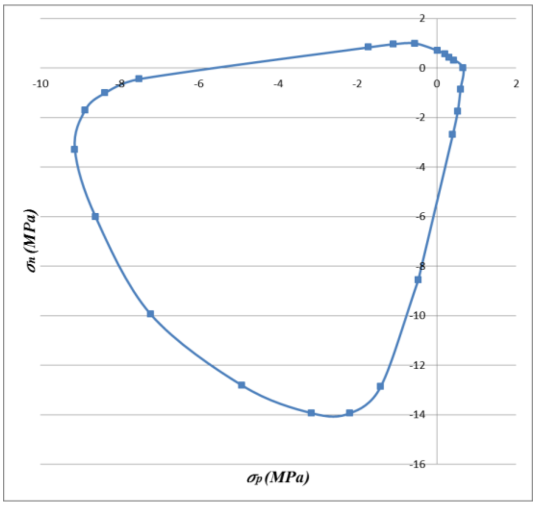

(b) P2

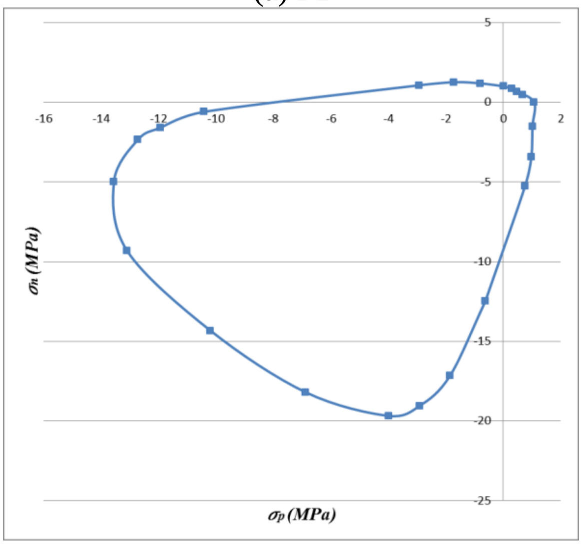

(c) P3

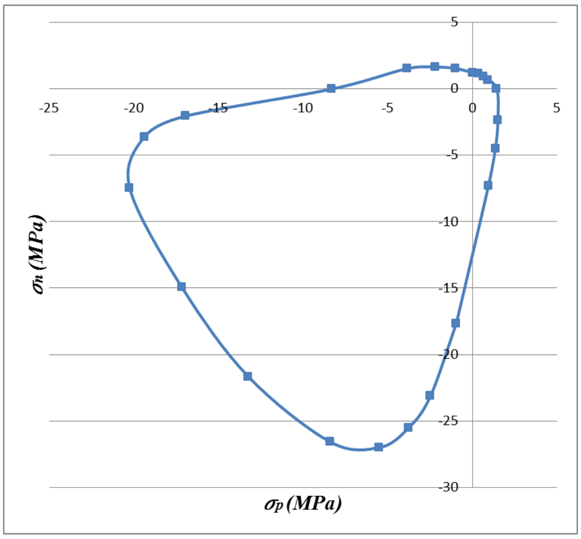

(d) P4

Figure 19: Biaxial failure envelope of the RVE in terms of principal stresses for concrete block masonry

The biaxial failure envelope of drystack masonry was also predicted using the RVE developed in Section 4.3 to validate the results of Oh et al, [37]. The RVE shown in Figure 11 was employed and simulated for different biaxial principal stress ratios shown in Table 8 for orientation angles of 0° and 90°, which represents the case of zero shear. The results are shown in Figure 20 for modified H-blocks and the interlocking drystack prisms.

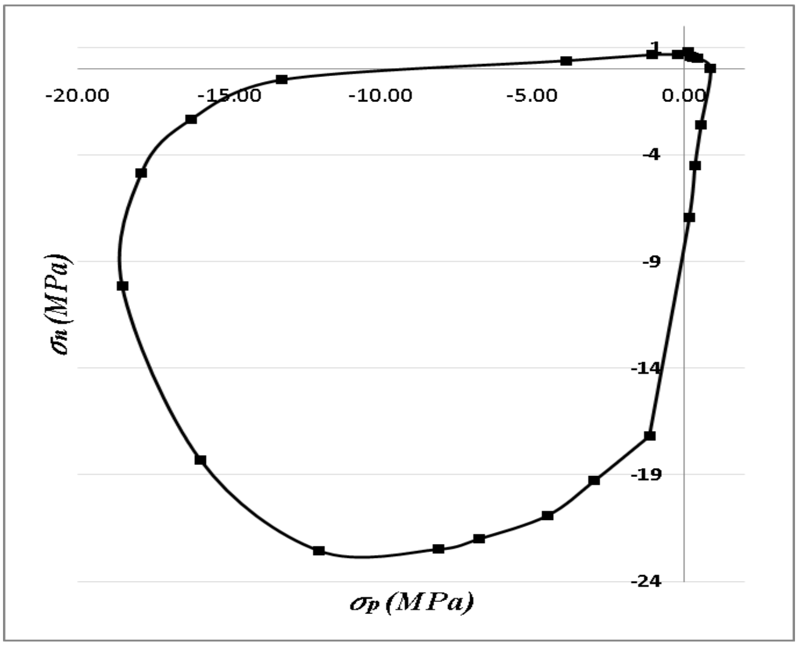

(a) Modified H-block prisms

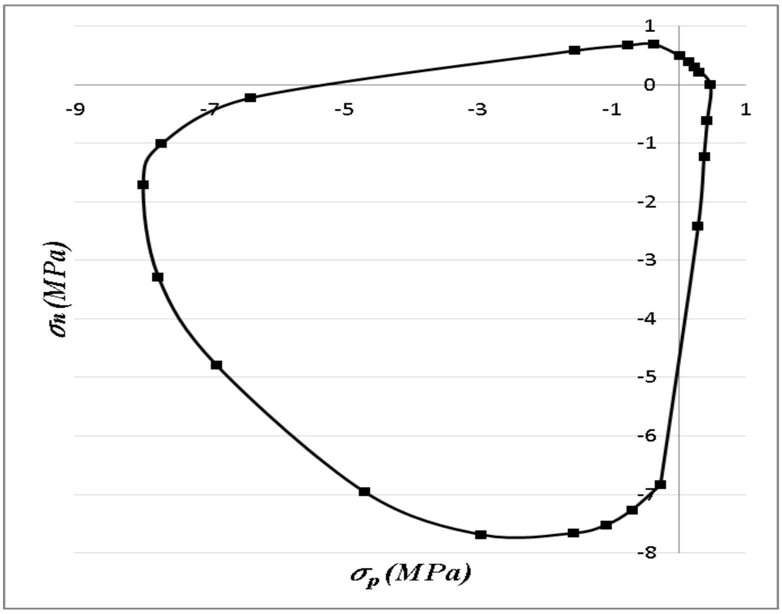

(b) Interlocking block prisms

Figure 20: Biaxial failure envelope of the RVE in terms of principal stresses for drystack masonry

Finally, to compare the biaxial failure of various masonry systems, the biaxial failure envelopes shown in Figures 16, 19 and 20 for clay brick, concrete block and drystack masonry respectively, were non-dimesionalised. Stresses in both orientations for all loading cases were divided by their respective unit strength to non-dimensionalise the ultimate strength of masonry. The mean strength of the units from each test is reported in Table 9.

These results are plotted in Figure 21 to depict the projection of strength in the σ_n - σ_p principal stress space.

Table 9: Mean strength of the units in different experiments

Reference	Mean Strength (f_u) (MPa)
Clay brick wallettes (Dhanasekar et al, [42])	15.41
Concrete Block prism, P1 (Barbosa et al, [36])	22.8
Concrete Block prism, P2 (Barbosa et al, [36])	18.6
Concrete Block prism, P3 (Barbosa et al, [36])	24.9
Concrete Block prism, P4 (Barbosa et al, [36])	36.2
Drystack H-block Prism, (Oh et al, [37])	30.7
Drystack Interlocking block Prism, (Oh et al, [37])	12.89

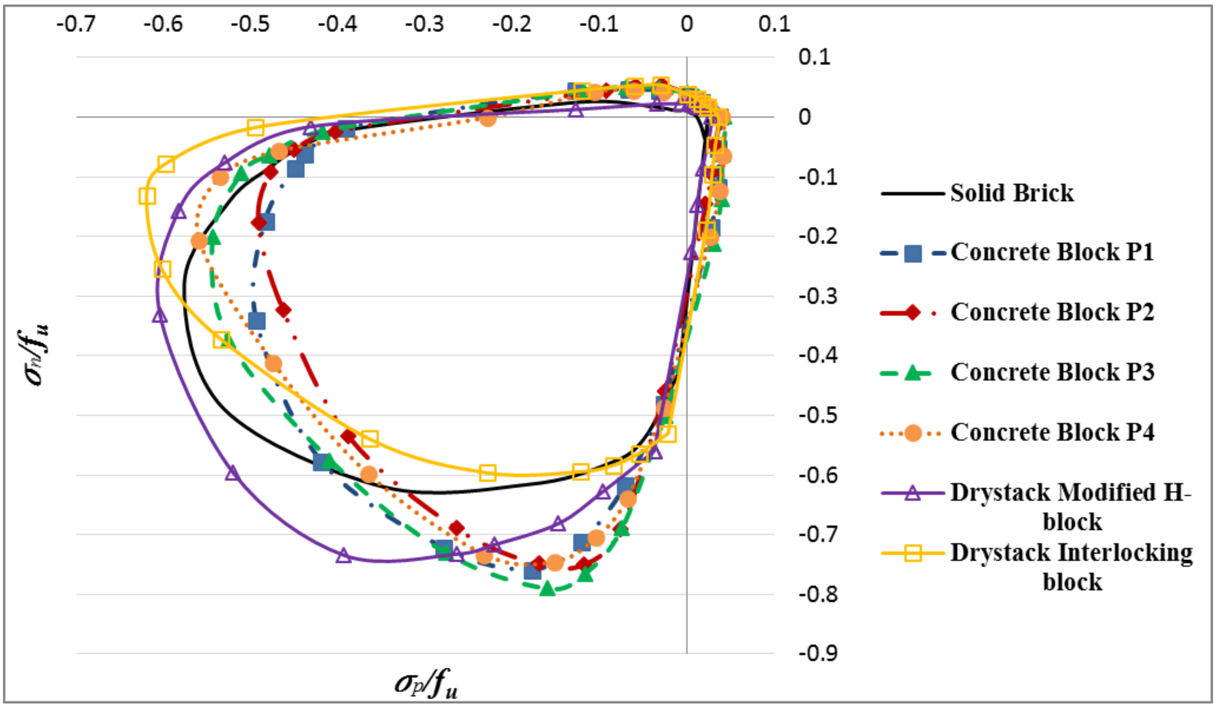

Figure 21: Combined biaxial failure envelopes of various types of masonry

The behaviour of all masonry types is quite similar, that is, higher strength in biaxial compression while very low strength in biaxial tension which is logical for masonry. From Figure 21 it can also be inferred that the failure envelope of the concrete block masonry has exhibited higher compressive strength than that of the clay brick masonry in the direction of perpendicular to the bed joint. In contrast, clay brick masonry has shown slightly higher failure strength for compression parallel to bed joint.

6- Conclusions and Observations

An interfacial transition zone (ITZ) enriched representative volume element (RVE) has been reported in this paper to predict the biaxial behaviour of various types of masonry. The ITZ was introduced between the two materials through several transition layers of varying thickness and degrading stiffness. Although the concept of ITZ is not new, the novelty of the formulation provided in this paper allows its application to combinations of weak mortar – strong unit (as in conventional masonry) and strong mortar – weak unit (as in high-bond strength masonry) to simulate the progressively damaging interface. By considering the interstices at the contacting interfaces between the dry-stacked blocks as a weak interface, the ITZ enriched RVE has also been shown to be effective in predicting the response of drystack (mortarless) masonry. The model was validated using three experimental datasets under uniaxial loadings for clay brick, concrete block and drystack masonry respectively. The validated RVEs for all of these types of masonry were then employed to predict the response of masonry subject to in-plane biaxial stress state for various loading ratios and bed joint angles. Good comparison between the model predictions and experimental data was obtained. Some specific conclusions from this study are:

- The ITZ enrichment with stiffness degrading properties between the masonry unit and mortar interface for a typical masonry RVE has been shown to predict the deformation and failure characteristics of masonry accurately without any need for interface elements or surface contact nonlinearities between the constituents.
- The developed ITZ enriched RVE is capable of predicting the uniaxial and biaxial failure envelope and deformation characteristics of various types of masonry including conventional clay brick, concrete block and drystack masonry accurately.
- Minimum thickness of the interphase (or, ITZ layer) should be at least 1.5mm to accurately predict the masonry behaviour.
- ITZ should be divided into a minimum of five layers of gradually degrading stiffness to simulate the damage in the unit-mortar interface.

The ITZ enriched RVE model analysis takes about 20-30 min of CPU time on a standard 3.4GHz, 8GB RAM desktop PC as an average, which is quite economical and comparable to macro-modelling of masonry. This RVE model can be employed in FE packages to analyse masonry walls and structures subjected to various in-plane loads without any need for complex contact nonlinearities or zero-thickness contact elements. Full-scale masonry walls can be analysed using the developed meso-scale RVE through multi-scale modelling technique. In the multi-scale modelling technique, full scale wall models are developed at a macro-scale with a course mesh incorporating a mesoscopic RVE (with finer mesh) to predict the material properties of masonry from the constituent materials (for example, brick and mortar). The properties of masonry are constantly updated consistent with the strain levels in the RVE (integration points) as predicted by the macro model of the modelled wall. This type of modelling will obviously be more expensive than a conventional FE model where the properties of masonry are directly tabulated. The advantage, however, is that there is no need for the analyst to know the properties of masonry as a priori – the properties are evaluated online from the basic properties of the constituents. In this way, overall, this modelling method can be regarded economical as complex experimental testing of masonry can be fully eliminated. The usefulness of the RVE for predicting out-of-plane response using layered shell element formulation to reproduce results in [46, 47] and for damage accumulation under seismic loading in [48-50] is being examined.

Acknowledgment

The authors would like to acknowledge Queensland University of Technology (QUT), Australia for providing high performance computing facilities to conduct this research.

References

[1] Jelvehpour, A., Zahra, T., and Dhanasekar, M., 2019. A non-local transient-gradient enhanced damage modelling method incorporating variable Poisson's ratio for brittle bi-material composites. Engineering Science and Technology, an International Journal, https://doi.org/10.1016/j.jestch.2019.05.007.

[2] Ramesh, G., Sotelino, E. D. and Chen, W. F., 1996. Effect of Transition Zone on Elastic Moduli of concrete materials. Cement and Concrete Research, 26(4): 611-622.

[3] Garboczi, E. J. and Bentz, D. P., 1997. Analytical formulas for interfacial transition zone properties. Advanced Cement Based Materials, 6(3-4): 99-108.

[4] Duplan, F. et al., 2014. Prediction of modulus of elasticity based on micromechanics theory and application to low-strength mortars. Const & Building Materials, 50: 437-447.

[5] Stroeven, M., Askes, H. and Sluys, L. J., 2004. Numerical determination of representative volumes for granular materials. Compu Meth in App Mech & Engg, 193(30-32): 3221-3238.

[6] Duan, H. L., Yi, X., Huang, Z. P. and Wang, J., 2007. A unified scheme for prediction of effective moduli of multiphase composites with interface effects. Part I: Theoretical framework. Mechanics of Materials, 39(1): 81-93.

[7] Lutz, M. P., Monteiro, P. J. M. and Zimmerman, R. W., 1997. Inhomogeneous Interfacial transition zone model for the bulk modulus of Mortar. Cement and Concrete Research, 27(7): 1113-1122.

[8] Nguyen, V. P., Lloberas-Valls, O., Stroeven, M. and Sluys, L. J., 2010. On the existence of representative volumes for softening quasi-brittle materials – A failure zone averaging scheme. Computer Methods in Applied Mechanics and Engineering, 199(45-48): 3028-3038.

[9] Klusemann, B. and Svendsen, B., 2012. Homogenization modeling of thin-layer-type microstructures. International Journal of Solids and Structures, 49(13): 1828-1838.

[10] Xu, W. X. and Chen, H. S., 2013. Analytical and modeling investigations of volume fraction of interfacial layers around ellipsoidal aggregate particles in multiphase materials. Modelling and Simulation in Materials Science and Engineering, 21(1).

[11] Nadeau, J. C., 2003. A multiscale model for effective moduli of concrete incorporating ITZ water–cement ratio gradients, aggregate size distributions, and entrapped voids. Cement and Concrete Research, 33(1): 103-113.

[12] Zheng, J., Zhou, X. and Jin, X., 2012. An n-layered spherical inclusion model for predicting the elastic moduli of concrete with inhomogeneous ITZ. Cement and Concrete Composites, 34(5): 716-723.

[13] Xiao, J., Li, W., Corr, D. J. and Shah, S. P., 2013. Effects of interfacial transition zones on the stress–strain behavior of modeled recycled aggregate concrete. Cement and Concrete Research, 52: 82-99.

[14] Zhou, C., Li, K. and Ma, F., 2014. Numerical and statistical analysis of elastic modulus of concrete as a three-phase heterogeneous composite. Computers & Structures, 39: 33-42.

[15] Mihai, I. C. and Jefferson, A. D., 2011. A material model for cementitious composite materials with an exterior point by microcrack initiation criterion. International Journal of Solids and Structures, 48(24): 3312-3325.

[16] Hatami-Marbini, H. and Shodja, H. M., 2008. On thermoelastic fields of a multi-phase inhomogeneity system with perfectly/imperfectly bonded interfaces. International Journal of Solids and Structures, 45(22-23): 5831-5843.

[17] Giambanco, G., and Mroz, Z.., 2001. The Interphase Model for the Analysis of Joints in Rock Masses and Masonry Structures. Meccanica 36: 111–130.

[18] Nazir, S., and Dhanasekar, M. 2013. Modelling the failure of thin layered mortar joints in masonry. Engineering Structures, 49: 615–627.

[19] Nazir, S., and Dhanasekar, M. 2014. A non-linear interface element model for thin layer high adhesive mortared masonry. Computers and Structures, 144: 23–39.

[20] Macorini, L., and Izzuddin, B. A. 2011. A non-linear interface element for 3D mesoscale analysis of brick-masonry structures. International Journal for Numerical Methods in Engineering, 85: 584–1608.

[21] Giambanco, G., Scimemi, G. F. and Spada, A., 2012. The Interphase finite element. Computational Mechanics, 50: 353-366.

[22] Scimemi, G., F., Giambanco, G., and Spada, A. 2014. The interphase model applied to the analysis of masonry structures. Computer Methods in Applied Mechanics and Engineering, 279; 66-85.

[23] Thamboo, J.A., Dhanasekar, M., and Cheng, Y. 2013. Effects of joint thickness adhesion and web shells to the face shell bedded concrete masonry loaded in compression. Australian Journal of Structural Engineering; 14(3): 291-302.

[24] Thamboo, J.A., Dhanasekar, M., and Cheng, Y. 2013. Flexural and shear bond characteristics of thin layer polymer cement mortared concrete masonry. Construction and Building Materials, 46: 104–113.

[25] Thamboo, J.A., and Dhanasekar, M. 2015. Characterisation of thin layer polymer cement mortared concrete masonry bond. Construction and Building Materials, 82: 71–80.

[26] Thamboo, J.A., Dhanasekar, M. 2016. Nonlinear Finite Element Modelling of High Bond Thin-Layer Mortared Concrete Masonry, International Journal of Masonry Research and Innovations. 1(1): 5-26.

[27] Zahra, T., and Dhanasekar, M. 2016. A generalised damage model for masonry under compression. International Journal of Damage Mechanics, 25(5): 629–660.

[28] Zahra, T., and Dhanasekar, M. 2018. Characterisation and strategies for mitigation of the contact surface unevenness in dry-stack masonry. Construction and Building Materials, 169: 612–628.

[29] Zahra, T., and Dhanasekar, M. 2016. Prediction of masonry compressive behaviour using a damage mechanics inspired modelling method. Construction and Building Materials, 109: 128–138.

[30] Caporale, A., Parisi, F., Asprone, D., Luciano, R., Prota, A. 2014. Critical surfaces for adobe masonry: micromechanical approach. Composites Part B: Engineering, 56:790-796.

[31] Parisi, F., Balestrieri, C., Varum, H. 2019. Nonlinear finite element model for traditional adobe masonry. Construction and Building Materials, 223:450-462.

[32] Augenti, N., Parisi, F. 2011. Constitutive modelling of tuff masonry in direct shear. Construction and Building Materials, 25(4):1612-1620. [4]

[33] Parisi, F., Balestrieri, C., Asprone, D. 2016. Nonlinear micromechanical model for tuff stone masonry: Experimental validation and performance limit states. Construction and Building Materials, 105:165-175.

[34] Dhanasekar, M., Page, A.W. and Kelleman, P.W. 1982, Finite element model for the inplane behaviour of brick masonry. Proc. 9th Australasian Conference on Mechanics of Materials and Structures, Sydney, Paper 7557.

[35] Thamboo, J.A. 2020. Material characterisation of thin layer mortared clay masonry. Construction and Building Materials 230:116932.

[36] Barbosa, C. S., Lourenco, P. B. and Hanai, J. B., 2010. On the compressive strength prediction for concrete masonry prisms. Materials and Structures, 43: 331-344.

[37] Oh, K.H., Harris, H.G. and Hamid, A.A. 1995. Behaviour of interlocking mortarless masonry under compressive loads. Proceedings of Seventh Canadian Masonry Symposium, Ontario, Canada. June 1995.

[38] Dhanasekar, M. 2011. Shear in reinforced and unreinforced masonry: Response, design and construction, Procedia Engineering, 14: 2069-2076.

[39] Han, J.J., and Dhanasekar, M. 2004. Modelling cracks in arbitrary shaped finite bodies using distributed dislocation, International J of Solids and Structures. 41(2): 399-411.

[40] Asad, M., Dhanasekar, M., Zahra, T. and Thambiratnam, D. 2019. Characterisation of polymer cement mortar composites containing carbon fibre or auxetic fabric overlays and inserts under flexure, Construction and Building materials, 224: 863-879.

[41] Grondin, F. and Matallah, M., 2014. How to consider the Interfacial Transition Zones in the finite element modelling of concrete? Cement and Concrete Research, 58, 67-75.

[42] Dhanasekar, M., Page, A. W. and Kleeman, P. W., 1985. Biaxial stress-strain relations for brick masonry. Journal of structural Engineering 111 (5): 1085-1100.

[43] Noor-E-Khuda, S., and Dhanasekar, M. 2017. Masonry Walls under Combined In-Plane and Out-of-Plane Loadings. Journal of Structural Engineering ASCE (2018) 10.1061/(ASCE)ST.1943-541X.0001930, 04017186.

[44] Noor-E-Khuda, S., Dhanasekar, M. and Thambiratnam, D.P. 2016, Out-of-plane deformation and failure of masonry walls with various forms of reinforcement, Composite Structures, 140: 262-277.

[45] Dhanasekar, M., Thamboo, J.A. and Nazir, S. 2017. On the in-plane shear response of the high bond strength concrete masonry. Materials and Structures, 50(5). DOI:10.1617/s11527-017-1078-7.

[46] Noor-E-Khuda, S., Dhanasekar, M., and Thambiratnam, D. P. 2016. An explicit finite element modelling method for masonry walls under out-of-plane loading. Engineering Structures, 113: 103–120.

[47] Noor-E-Khuda, S., and Dhanasekar, M. 2020. On the out-of-plane flexural design of reinforced masonry walls. Journal of Building Engineering, 27: 100945.

[48] Dhanasekar, M. and Shrive, N.G. 2002, Strength and deformation of confined and unconfined grouted concrete masonry, ACI Structural Journal, 99(6): 819-826.

[49] Kreiser, D., Jia, S.X., Han, J.J. and Dhanasekar, M. 2007, A nonlinear damage accumulation model for shakedown failure, International Journal of Fatigue, 29(8): 1523-1530.

[50] Thamboo, J.A., Zahra, T. and Dhanasekar, R. 2020. Development of design methodology for mortarless masonry system: Case study – a resettlement housing colony. Journal of Building Engineering, 27: 100973.